Numerical modeling with experimental verification investigating the effects of nonlinearities on the sideband peak count-index technique and topological acoustic sensing

Guangdong Zhang<sup>1, 2, 3</sup>, Bo Hu<sup>4</sup>, Hamad Alnuaimi<sup>5</sup>, Umar Amjad<sup>6</sup>, Pierre A. Deymier<sup>1, 7</sup>, Keith Runge<sup>1, 7</sup> and Tribikram Kundu<sup>1, 2, 4, 7, \*</sup>

- 1. New Frontiers of Sound Science and Technology Center, University of Arizona, Tucson, AZ, 85721, USA.
- 2. Department of Civil and Architecture Engineering and Mechanics, University of Arizona, Tucson, AZ, 85721, USA.
- 3. School of Traffic and Transportation Engineering, Central South University, Changsha, Hunan, 410075, China.
- 4. Department of Aerospace and Mechanical Engineering, University of Arizona, Tucson, AZ, 85721, USA.
- 5. Department of Civil and Architectural Engineering, Qatar University, Doha, Qatar.
- 6. Center for Advanced Materials, Qatar University, Doha, Qatar.
- 7. Department of Materials Science and Engineering, University of Arizona, Tucson, AZ, 85721, USA.

\*Corresponding author: tkundu@arizona.edu

Abstract: A newly developed nonlinear ultrasonic (NLU) technique called sideband peak count-index (or SPC-I) measures the degree of nonlinearity in materials by counting the sideband peaks above a moving threshold line – larger the SPC-I value, higher is the material nonlinearity. In various published papers, the SPC-I technique has shown its effectiveness in structural health monitoring (SHM) applications. However, the effects of different types of nonlinear phenomenon on the sideband peak generation is yet to be investigated in depth. This work addresses this knowledge gap and investigates the effects of different types of nonlinearity on the SPC-I technique. Three types of nonlinearity (material nonlinearity, structural nonlinearity and contact nonlinearity) are investigated separately through numerical

modeling. Numerical modeling results show that the sideband peak values do not increase proportional to the input signal strength thus indicating nonlinear response, and different types of nonlinearities affect the SPC-I measurements differently. For the experimental verification a composite plate with impact-induced damage is considered for investigating the material nonlinearity and structural nonlinearity while a linear elastic aluminum plate is used to examine the contact nonlinearity between the transducers and the plate. The trends observed in the experimental observations matched the numerical model predictions. Monitoring damage growth in topographical structures – formed by inserting different materials in a matrix material is also investigated. In addition to the SPC-I technique an emerging acoustic parameter – "geometric phase change" based on the topological acoustics is also adopted for sensing damage growth in the topographical structures. The performance of SPC-I and topological acoustic sensing techniques as well as the spectral amplitude difference (SAD) parameter for sensing the damage growth in topographical structures are compared and discussed.

**Keywords:** Structural health monitoring, nonlinear ultrasonic technique, SPC-I technique, numerical modeling, topological acoustic sensing, geometric phase change, spectral amplitude difference

#### 1. Introduction

Ultrasonic nondestructive testing and evaluation (UNDT&E) techniques are widely used in structural health monitoring (SHM) applications. In recent decades, nonlinear ultrasonic (NLU) techniques have become increasingly popular for their high sensitivities compared to traditional linear ultrasonic (LU) techniques [1]. A newly developed NLU technique called sideband peak count-index (or SPC-I) has shown promising results for damage monitoring in various materials. In the existing literature one can see that the SPC-I value indicates the degree of nonlinearity in a specimen [2]. However, as an emerging NLU technique, it is crucial to investigate the nonlinear mechanism or phenomenon that causes the variation of SPC-I values. This aspect has not been reported or investigated in depth yet for this new NLU technique. Having a deep insight into the nonlinear phenomenon generation can provide the evidence for the effectiveness of the SPC-I technique by understanding the mechanism of SPC-I better.

The newly developed SPC-I technique shows some advantages over other NLU techniques such as the two most popular techniques – higher harmonic generation (HHG) technique and the nonlinear wave modulation spectroscopy (NWMS) method or frequency modulation (FM) method. For example, when adopting the HHG technique for guided waves propagating in plate structures, the guided wave mode selection criterion requires phase velocity and group velocity matching conditions [3, 4]. Even for P-waves propagating in simple bulk structures, uniform propagation paths between the transmitter and the receiver are required, and an interface or a complex geometry can distort the harmonics and make the technique harder to apply [2]. Moreover, when waves propagate in highly attenuated materials such as composite materials, generated higher harmonic components cannot be extracted successfully due to high material attenuation. A method called static component (SC) can help overcome the mentioned drawbacks with low attenuation for low frequency or quasi static component waves and be used to monitor damages in highly attenuated composite materials [5-7]. The NWMS/FM technique can be applied regardless of the material geometry or the presence of

reflecting boundaries and structural inhomogeneity. However, the two input wave frequencies for wave mixing need to be precisely controlled for optimal sideband generation, which means narrow band excitation is needed [1, 8]. The SPC-I technique does not have such restrictions and hence easier to implement compared to the above mentioned popular NLU techniques. In the SPC-I technique, sideband peaks are counted above a moving horizontal threshold line as this line varies between a preset lower limit and an upper limit in the spectral plots [9]. The SPC-I value is the average of all these peak counts. Larger the SPC-I value, higher is the material nonlinearity. Based on this basic principle, many experimental investigations have been conducted with the SPC-I technique, including the degradation monitoring of concretes [10-13], impact-induced damage monitoring in composites [2, 14, 15], elastoplastic deformation and fatigue crack growth monitoring in metallic materials [8, 16], porosity monitoring in additively manufactured components [17] and so on. In all those experimental investigations, the SPC-I values have shown promising results for damage, crack or pore volume monitoring, thus showing potential applications of the SPC-I technique for structural health monitoring.

For nonlinear wave propagation modeling, the SPC-I technique is adopted to extract the nonlinear interactions between cracks and elastic waves. This technique also gives promising results for monitoring cracks. For instance, Hafezi and Kundu et al [18-20] investigated the nonlinear wave propagation interacting with single crack in two-dimensional (2-D) structures using nonlocal bond-based peridynamics (or peri-ultrasound modeling) and found that the SPC-I shows larger values for thin cracks than thick cracks and no crack cases. Zhang et al [21, 22] adopted ordinary state-based peri-ultrasound theory for modeling nonlinear wave propagation interacting with multiple cracks in three-dimensional (3-D) plate structures. They showed the relation between the horizon size which is used in peridynamics theory and the crack dimensions. The SPC-I technique was adopted to extract the nonlinear response and found similar trends – larger SPC-I values for thin cracks than thick cracks and no crack cases.

Because of the flexibility of the SPC-I technique, it has been also adopted to monitor dynamic crack propagation process in plate structures combining both peridynamics and peri-ultrasound modeling [23]. It showed that the SPC-I values increased as the external loading time of the crack propagation increased, and then decreased. This is because nonlinear SPC-I is sensitive to micro-cracks which are generated at the early stages of crack propagation. Then these microcracks coalesce to form macro-cracks as the loading time increases thus causing a decreasing trend of the SPC-I value. This finding matches with the experimental observation [2, 16]. These investigations based on numerical modeling with some experimental verifications show the potential advantages of this newly developed NLU technique. It must be mentioned here that the numerical modeling method – ordinary state-based (OSB) peri-ultrasound modeling developed in references [18] and [19] is also adopted in this paper for structural nonlinearity (crack-induced nonlinearity) investigation. Numerical modeling methods for nonlinear waves propagating in structures and interacting with cracks are meager. The peri-ultrasound modeling shows advantages of modeling nonlinear waves interacting with cracks over other numerical methods such as modified finite element method (FEM) – activation/deactivation of elements approaches [24], spring model [25] and other advanced numerical modeling methods such as finite difference based local interaction simulation approach (LISA) [26, 27]. In these numerical methods the cracks' surface properties need to be changed artificially, but it is not necessary in the nonlocal peri-ultrasound modeling since the wave energy can still pass through finite thickness cracks due to the nonlocal effect.

Though success stories of SPC-I for both experimental and numerical modeling investigations have been reported in the literatures some knowledge gap still exists. The problem of how the nonlinear phenomenon or mechanism affects the SPC-I technique has not been extensively addressed. For example, in an engineering material like concrete, due to the inherent inhomogeneity one knows that the sideband peaks appear in the spectral plots. However, when the degree of damage in the same sample increases, whether the amplitude

variations of the sideband peaks (away from the central frequency) and the main peaks (around the central frequency range) are due to linear mechanism like wave scattering or due to some nonlinear mechanism has not been properly addressed yet. If these sideband peak amplitudes change in a purely linear manner as the main peak amplitudes do, then the SPC-I technique should not be called a nonlinear technique, since then it simply measures linear scatterings by internal damages. However, if one can show that these sideband peak amplitudes change in a nonlinear manner while the main peak amplitudes change linearly when the degree of nonlinearity varies, then it can be stated that the SPC-I technique measures the nonlinear phenomenon or mechanism.

In light of the above discussion, both numerical modeling and experimental investigations are conducted to examine the generation of sideband peaks due to three different types of nonlinearity – material nonlinearity, structural nonlinearity and contact nonlinearity. In numerical modeling part, the material nonlinearity is modeled by the finite element method (FEM) using commercial software Abaqus/CAE considering different types of stress-strain relations; the structural nonlinearity which is commonly related to the breathing phenomenon of cracks in structures is achieved with peri-ultrasound modeling by taking the advantage of the nonlocal interactions. Finally the transducer-structure contact nonlinearity is modeled using Abaqus finite element software. In experimental part, one composite plate containing impact-induced cracks is used to investigate the effect of the material nonlinearity and the structural nonlinearity, while an isotropic damage-free aluminum plate is used to study the contact nonlinearity.

Damage growth in topographical structures formed by inserting thin strips made of a different material than the plate material or the matrix material is also investigated using the SPC-I technique. Another emerging acoustic parameter – geometric phase change derived from topological acoustics is also adopted for sensing damage growth in topographical structures. Performances of the nonlinear technique SPC-I, linear technique spectral amplitude difference

(SAD) and topological acoustic sensing technique geometric phase change are compared for damage monitoring in topographical structures.

## 2. Model description for numerical modeling

In this section, three types of nonlinearity – material nonlinearity, structural nonlinearity and contact nonlinearity are investigated using two different numerical modeling methods. The material nonlinearity and contact nonlinearity investigations are conducted with finite element method (FEM) using commercial Abaqus/CAE software, and the structural nonlinearity problem is modeled by the nonlocal peri-ultrasound modeling technique.

#### 2.1 Material nonlinearity in plate structures

The 2-D view (the xy plane) of the problem geometry for material nonlinearity investigation is shown in figure 1a. The dimension of the plate structure is  $200 \times 200 \times 3 \text{mm}^3$ , and the material properties for numerical modeling are listed in Table 1. For wave propagation setup, the transmitting point and the receiving point are selected on the top surface of the plate along the y-axis, and distributed symmetrically about the x-axis. The vertical distances from both the transmitting point and the receiving point to the x-axis are 60 mm.

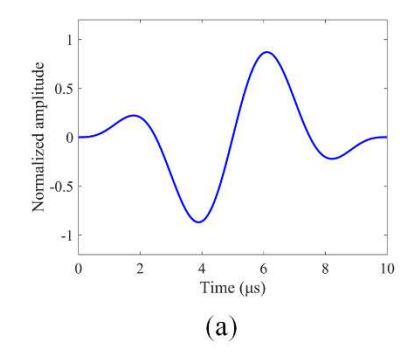
Material parameters Young's modulus (GPa) Poisson's ratio Density (kg/m³) 71.50 0.33 2700 Values 200 Linear Square root 150 120 MPa Stress (MPa) 90 MPa 100 30 MPa 0.5 1.5 Strain  $\times 10^{-3}$ 

Table 1. Material properties for numerical modeling.

Figure 1. 2-D view of the problem geometry and stress-strain relations for wave propagation modeling.

To investigate the generation of sideband peaks in the SPC-I technique, two different stress-strain relations are considered for the numerical modeling. As shown in figure 1b, the solid line indicates a linear stress-strain relation where the stiffness remains constant; the dotted line shows a square root stress-strain relation where the stiffness decreases as load increases. The marked three numbers on each curve prescribe the amplitude of the input ultrasonic wave when loaded along the assumed stress-strain relation lines. Amplification factors (AF) are defined as the ratio of any amplitude to the initial amplitude (since we are interested in a monotonous trend of the input or initial loading the initial amplitude can either be the largest or the smallest value. Typically, it is the minimum value in this research). For the top line these numbers are 40 MPa for the initial amplitude and then the amplitude is increased to 80 MPa which corresponds to an amplification factor (AF) of 2 (80 divided by 40). Similarly, the amplitude 120 MPa on the top line corresponds to AF equal to 3, and of course the 40 MPa itself is with AF equal to 1. The AF values for the bottom solid curve are defined in the same manner and also taken as 1, 2 and 3.

The normalized time domain and frequency domain signals for the input or initial excitation are shown in figure 2. The central frequency of the initial excitation is 200 kHz. A Hanning window is adopted to modulate the two cycles to improve the signal resolution at the receiving point.



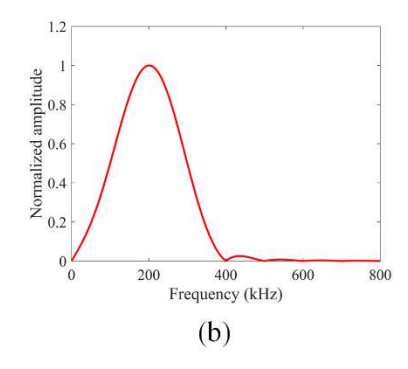


Figure 2. Normalized input or initial excitation. (a) Time domain signal and (b) frequency domain signal.

The entire 3-D plate structure is discretized using elements having a side length of 1 mm.

Such discretization produces 201 nodes along the x-axis thus making both transmitting and receiving points located on the central line (y-axis) of the plate structures and other nodes are distributed symmetrically about the y-axis. A dynamic explicit solution scheme is adopted for our calculation. The initial excitation is applied on the transmitting point in the negative z direction, and out-of-plane velocity fields are recorded at the receiving point for further analysis. The sampling frequency at the receiving point is 50 MSa/s (mega samples or mega points per second). For each stress-strain relation shown in figure 1b there are three recorded signals which correspond to the AF values equal to 1, 2 and 3, respectively, so a total of six signals are recorded for the material nonlinearity analysis.

## 2.2 Structural nonlinearity in plate structures

Structural nonlinearity is generated by breathing cracks in a linear material. Since opposing surfaces of thin cracks can relatively easily come in contact in comparison to thicker cracks when elastic waves propagate through the cracks, the thinner cracks show higher nonlinearity. Here, we adopt the nonlocal ordinary state-based peri-ultrasound modeling technique to model elastic waves interacting with preset cracks and thus producing the structural nonlinearity. The detailed description of the adopted peri-ultrasound modeling can be found in first and last authors' previously published papers [21, 22], and here we simply describe the problem geometry and the wave propagation setup omitting the detailed calculation process description. In this modeling, two cracks are considered for the structural nonlinearity investigation and the 2-D view of the problem geometry is shown in figure 3. The dimension of the plate structure is  $201 \times 201 \times 3 \text{mm}^3$ . The vertical distances from the transmitting point and the receiving point to the x-axis are 60 mm, and the transmitting point and the receiving point are located on the y-axis symmetrically about the x-axis. Two cracks with length 19 mm and width d equal to 2 mm are introduced. The two cracks are symmetrically placed about the x-axis and the closest vertical distances from the x axis to the surface of the two cracks are 20 mm as shown in figure 3.

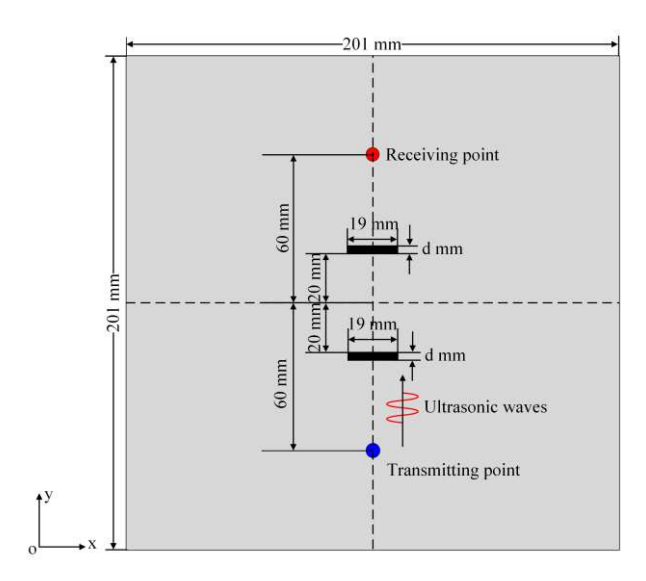


Figure 3. 2-D view of the problem geometry of the plate structure for structural nonlinearity modeling due to wave-crack interaction.

In the mesh-free peridynamics based peri-ultrasound modeling the entire plate structure is discretized into cubes with side length 1 mm, therefore, 201 cubes are formed in the x direction with the problem geometry shown in figure 3. All output variables are recorded on particles at receiving locations which are located along the central line (y-axis) of the plate structures with other particles distributing symmetrically about the y-axis, and this is consistent with what is done in the finite element modeling in section 2.1. Cracks are formed by removing one or more layers of cubes from the plate structure. Each crack in figure 3 is formed by removing 2 layers of cubes in the y direction and in each layer 19 cubes in the x direction are removed. The normalized input signal is the same as shown in figure 2 in section 2.1, but the minimum amplitude of the excitation in peri-ultrasound modeling is set as  $1 \times 10^{-5}$  m. The AF values considered here are also different, which are multiple times of this amplitude. Out-of-plane velocity fields at the receiving point are recorded for further analysis. The AF values of 1, 10, 20 and 50 are considered for the investigation of sideband peak generation for this problem geometry.

#### 2.3 Transducer-specimen contact nonlinearity

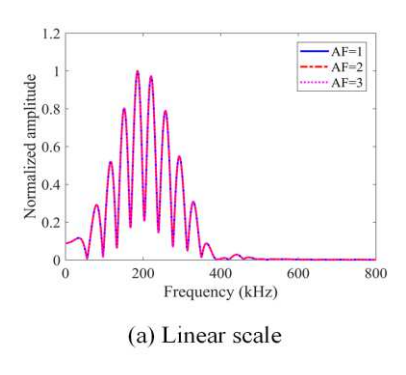
The problem geometry of the plate structure for this investigation is the same as that in section 2.1, but the main difference is that instead of applying the initial excitation directly at the transmitting point, a small block with dimension  $4 \times 4 \times 2 \text{mm}^3$  is attached at the transmitting location. The contact between the bottom surface of the block and the top surface of the plate is set as "hard contact" in the Abaqus software. For the hard contact the bottom surface of the block is set as the master surface and the top surface of the plate structure in the contact region is set as the slave surface since wave energy propagates from the block to the plate structure. When the two surfaces are in contact (interface gap is less than zero), all fields such as normal and shear stress components and displacement components satisfy continuity conditions as waves propagate across the contact interface. However, when the interface gap is larger than or equal to zero (two faces are separated), the stress and displacement fields cannot pass through the interface. Therefore, the "hard contact" cannot transfer the tensile stress. It can be effectively used to model contact interface avoiding penetration but allowing possible separation between two surfaces in contact. It is appropriate to model the scenario when mechanical energy from PZT (Lead zirconate titanate) transducers transfers to structures. The initial excitation or the input excitation of the ultrasonic wave is applied on the top surface of the block in the negative z direction. The material properties and wave propagation parameters are kept the same as in section 2.1. Received signals when AF is equal to 1, 10 and 50 are recorded to investigate how contact influences the sideband peak generation.

#### 3. Results of numerical modeling

As mentioned in the introduction part, the main interest of this work is to investigate how sideband peak amplitudes change as the initial excitation amplitude increases when wave propagates through various types of nonlinearity. Therefore, in this work one only needs to examine how sideband peaks change in the spectral plots. All spectral results from the recorded data in section 2 are shown and analyzed in this section.

#### 3.1 Influence of material nonlinearity on sideband peak generation

The normalized spectral plots for the two different stress-strain relations are shown in figures 4 and 5, in both linear scale and logarithmic scale. It is plotted in both linear and logarithmic scales to clearly show how material nonlinearity affects the main band and the side bands. Figures 4 and 5 correspond to linear and nonlinear stress-strain relations, respectively.



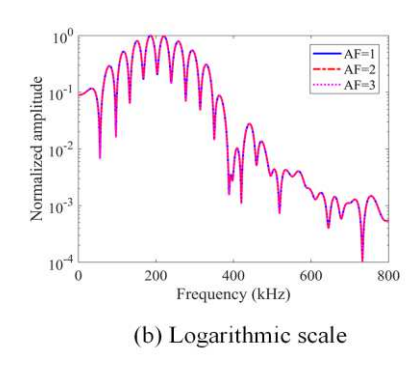
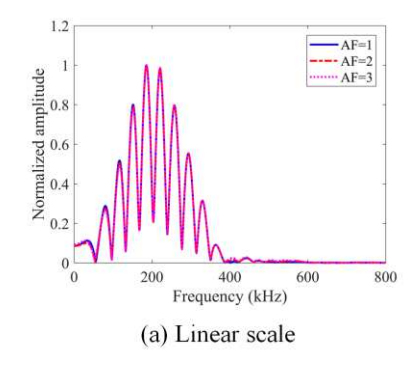


Figure 4. Normalized spectral plots in both linear scale and logarithmic scale for different AF values for linear stress-strain relation.



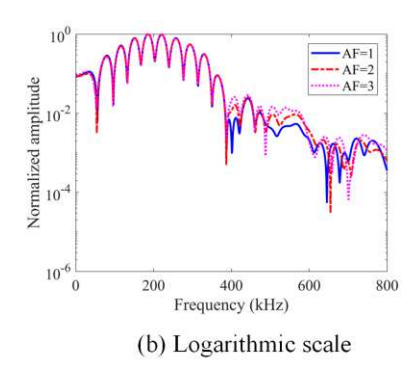


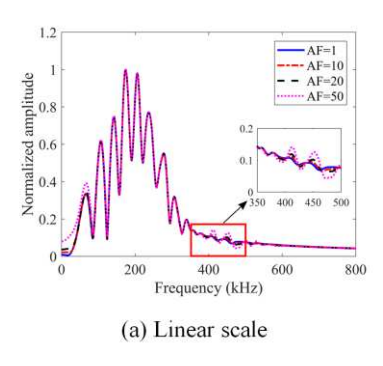
Figure 5. Normalized spectral plots in both linear scale and logarithmic scale for different AF values for nonlinear stress-strain relation.

It can be seen in figure 4 that for linear stress-strain relation both the main peaks (lobes around the central frequency 200 kHz) and the sideband peaks (which are further away from the 200 kHz central frequency) are showing no difference for different AF values in these normalized plots. This is because all peaks are increasing in a linear manner for linear stress-strain relation; hence when the input signal is amplified by a factor of 2 or 3 the entire response

is amplified by the same factor, and hence there is no difference in the normalized plots for AF equal to 1, 2 and 3. For nonlinear stress-strain relation, as can be seen in figure 5 the sideband peaks show nonlinearity – sideband peak amplitudes increase as the AF increases while the main lobe amplitudes do not change in the normalized plots. Variations in the sideband peak amplitude values in the normalized plots is due to the material nonlinearity. Thus, it is clearly shown here that the main lobes near the central frequency cannot detect nonlinear stress-strain relation but the sidebands away from the central frequency can do that. These numerical results suggest that variations of sideband peak amplitude values in normalized plots indicate material nonlinearity but the peaks in the main lobe are insensitive to it. Therefore, variations in the SPC-I values can be related to the variations in the material nonlinearity.

## 3.2 Influence of structural nonlinearity on sideband peak generation

Normalized spectral plots for structural nonlinearity investigation are shown in figure 6 in both linear and logarithmic scales.



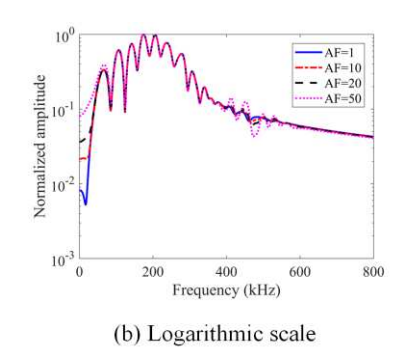


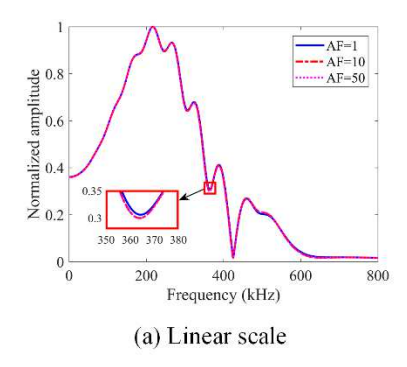
Figure 6. Normalized spectral plots in (a) linear scale and (b) logarithmic scale for different AF values.

It can be seen from figure 6 that as the AF values increase the main lobes which are near 200 kHz frequency do not change which indicate linear behavior. Sideband peaks, however, behave in nonlinear manners at high frequency ranges (more obvious between 350 kHz and 500 kHz). The evidence provided here proves that the SPC-I technique which is derived from the sideband peak counts to varying thresholds indeed captures nonlinear response of structures. Since here the nonlinearity is introduced only through breathing effect of cracks, while the

material is linear the variations in the sidebands are much smaller in figure 6 compared to figure 5 where the entire plate is made of nonlinear material.

#### 3.3 Influence of contact nonlinearity on sideband peak generation

Similarly, in figure 7 we plot the normalized spectral plots in both linear and logarithmic scales for contact nonlinearity case.



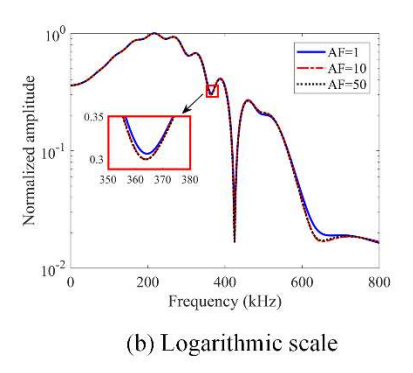


Figure 7. Normalized spectral plots in (a) linear scale and (b) logarithmic scale for different AF values for transducer-structure contact nonlinearity.

It can be seen from figure 7 that sideband peak amplitudes show a decreasing trend at some high-frequency ranges as AF values increase. This trend will be investigated experimentally in section 4. One can also see that the nonlinear response is quite small even for a large AF value. Hence, such transducer-specimen contact nonlinearity effect can be ignored in structural health monitoring applications.

#### 4. Experimental results

In sections 2 and 3, effects of three types of nonlinearity on the sideband peak generation have been investigated numerically. In this section experimental results are presented. First, the experimental setup and the process are illustrated, and then experimental results for these three nonlinear scenarios are shown. Finally, a comparison between experimental results and numerically generated results are presented.

## 4.1 Experimental setup

The ultrasonic testing experimental setup is illustrated in figure 8 and is adopted from the

first and last authors' recently published paper [28]. It shows a photograph (figure 8a) and a schematic diagram (figure 8b) of the experimental setup. A computer controlled arbitrary function generator is employed to generate electric pulses, which are amplified by an amplifier and then converted to ultrasonic pulse by a PZT sensor, serving as the excitation source in the experimental setup. The ultrasonic pulse travels through the plate specimen. At the receiving end the ultrasonic pulse is detected and then converted back to an electric signal by a second PZT sensor. The PZT sensors are attached to the plate specimens for the purpose of generating and propagating guided waves in the plate.

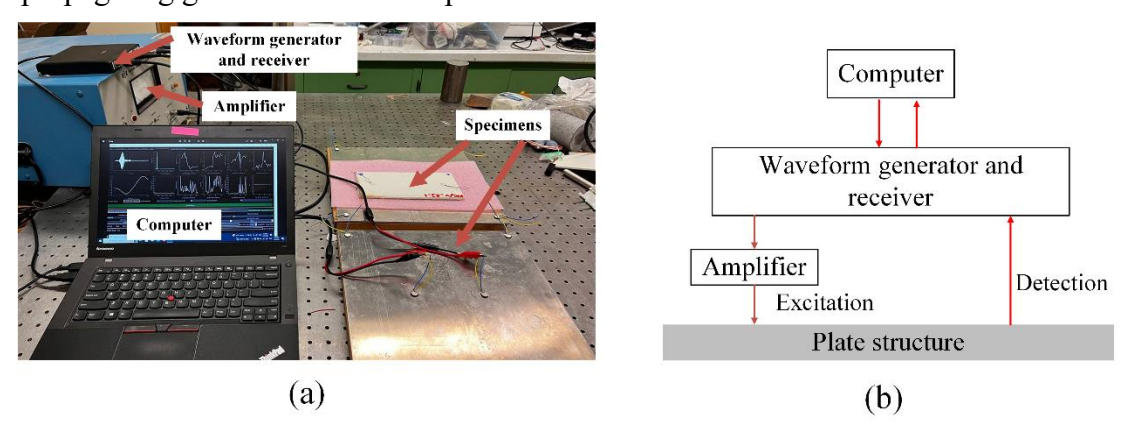


Figure 8. (a) The photograph and (b) the schematic diagram of the ultrasonic test setup [28].

Two plate structures — one composite plate and one aluminum plate are used in the experiment. The composite plate was impacted at the center causing cracks in the central region. One should note that both material nonlinearity and structural nonlinearity are present in this composite plate. In general, polymer composite materials have some inherent nonlinear stress-strain relations thus when elastic waves propagate through a polymer composite plate then material nonlinearity affects the propagating waves. In this case, impact-induced cracks also introduce some structural nonlinearity. Then a similar experiment is carried out on an aluminum plate to investigate how the transducer-specimen contact affects the sideband peak generation. For the aluminum plate the material is linear and there is no other nonlinearity introduced in the structure, hence if any nonlinearity is observed then it must be from the contact at the

transducer-plate interface. We are only interested here in investigating how sideband peak amplitudes vary with input signal amplitude variation. For both composite and aluminum plates different initial excitation voltages are used, and detected signals at the receiver are stored for further signal processing.

## 4.2 Experimental results and analysis

#### 4.2.1 Material and structural nonlinearity

As we mentioned in section 4.1 a composite plate with impact induced cracks has both material nonlinearity and structural nonlinearity. The inherent nonlinear stress-strain relations in polymer composite materials which affect the wave propagation is referred as material nonlinearity while the impact generated cracks introduce structural nonlinearity in the plate structure. In this case, waves propagate through the composite plate and are detected by the sensor are affected by both the material nonlinearity and the structural nonlinearity; the normalized spectral plots in both linear and logarithmic scales are shown in figure 9.

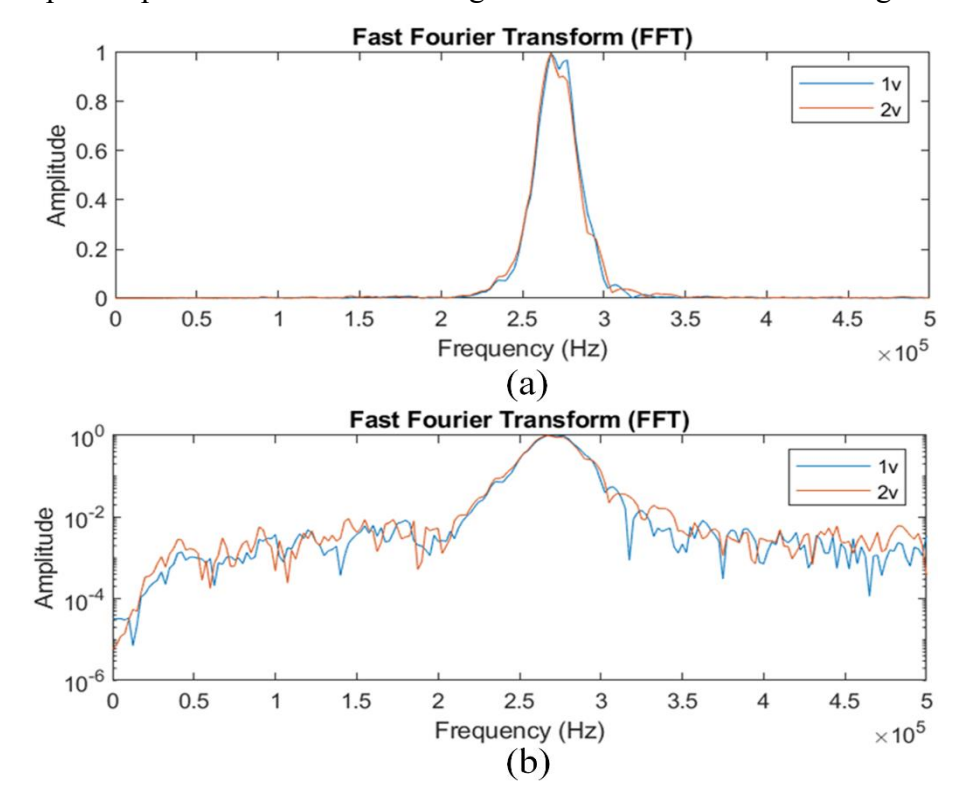


Figure 9. Normalized spectral plots in (a) linear and (b) logarithmic scales for 2 different excitations [28].

It can be seen from figure 9 that when the input signal voltage increases from 1 V to 2 V (so AF values are equal to 1 and 2) the main lobe amplitudes which are between 250 kHz and 280 kHz remain approximately the same in the normalized plots while sideband peak amplitudes show an increasing trend indicating a nonlinear behavior. These observations are consistent with the results generated numerically in the investigation of material nonlinearity in section 3.1, thus it verifies the numerical modeling results.

# 4.2.2 Transducer-specimen contact nonlinearity

The normalized spectral plots for detected signals in the aluminum plate in both linear and logarithmic scales are shown in figure 10.

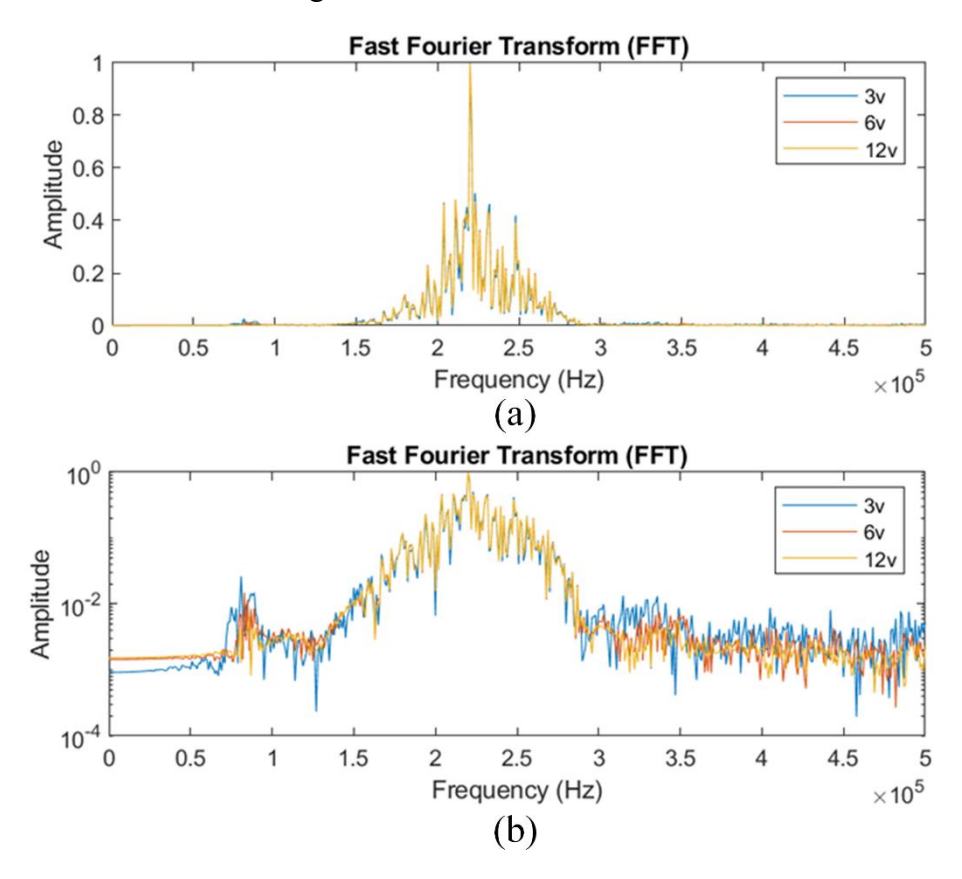


Figure 10. Normalized spectral plots in (a) linear scale and (b) logarithmic scale for 3 different initial excitation amplitudes [28].

Figure 10 shows sideband peak amplitude decreasing as the input signal voltage increases

similar to the numerical model predictions. Clearly, transducer-specimen contact nonlinearity behaves differently than material and structural nonlinearities. Moreover, it can be seen that when the input excitation amplitude increases from 3 V to 6 V, the changes in sideband peak amplitudes are significant. However, changes in sideband peak amplitudes are small when voltage increases from 6 V to 12 V. Similar phenomena is also observed in the numerical modeling results in figure 7 that when the AF value increases from 1 to 10 the changes for sideband peak amplitudes are larger than when it increased from 10 to 50. From both numerical modeling and experimental results one can conclude that the contact nonlinearity effect diminishes for larger input excitations. One should note that the central frequency of the recorded signals in the experiment is slightly more than 200 kHz and is not strictly matching the central frequency used in the numerical modeling. This is because the transducers' central frequency was not exactly what was specified by the transducer manufacturer. However, the main interest of this work is to investigate the effect of excitation amplitude on the sideband peak generation and such slight frequency difference should not make much difference in the qualitative comparison carried out here between the numerical and the experimental results.

#### 5. Monitoring damage growth in topographical structures by the SPC-I technique

So far, both numerical modeling and experimental results show that the SPC-I technique can capture the nonlinear response and is not simply recording the linear scattering. In this section we adopted the SPC-I technique for monitoring damage growth in topographical structures. Topographical structures are formed by inserting strips of different materials from the matrix material and thus making the structure heterogeneous. Such heterogeneous structures complicate the wave propagation. At certain points destructive interference between incident, reflected and transmitted elastic waves can make those points insensitive to the damage growth when adopting acoustics based structural health monitoring (SHM) techniques. Here, investigations are carried out to check the effect of topography on damage growth monitoring by the SPC-I technique. The spectral amplitude difference (SAD) parameter is also

used for damage growth monitoring and compared with the SPC-I predicitions.

## 5.1 Model description for damage growth

Plate structures containing two identical cracks in a heterogeneous plate (due to topography) and in a homogeneous plate (having no topography) are investigated and compared to examine the effect of topography on the detectability of cracks in such plate structures using the SPC-I technique. For the homogeneous plate or no-topography case, an isotropic aluminum plate is considered and the 2-D view of the problem geometry is shown in figure 11a. Then topographical structures are formed by inserting thin strips of steel in the aluminum plate, thus the topographical structure becomes heterogeneous. We call it "X" topography indicating that these strips are arranged along x-axis; the 2-D view of the problem geometry is shown in figure 11b. The "X" topography shown in figure 11b consists of two pairs of steel strips (a total of four strips) inserted in the aluminum plate. Both pairs of strips are symmetrically arranged about the y-axis. The width of the strips is 7 mm and their length is 201 mm.

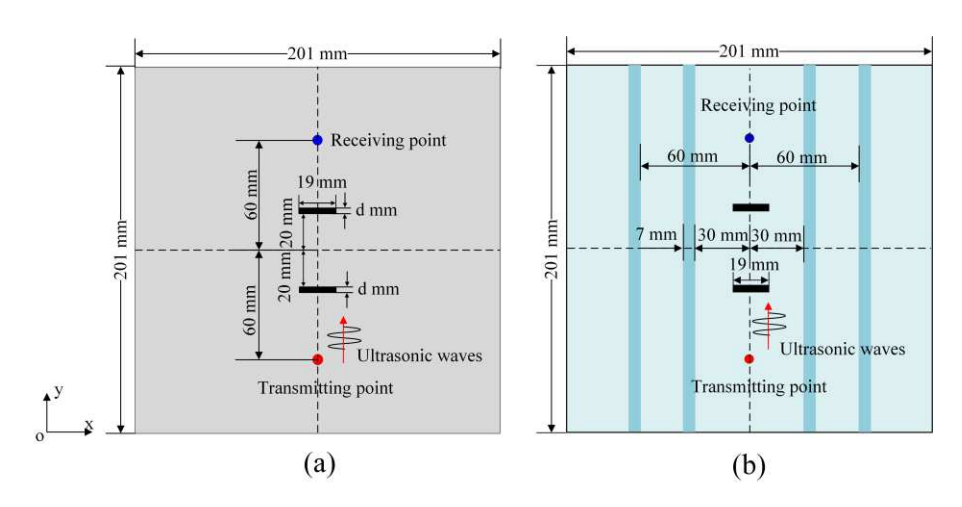


Figure 11. 2-D view of problem geometry of homogeneous and heterogeneous plate structures containing cracks (a) homogeneous plate and (b) "X" topography in the plate.

The dimension of the plate structure is 201×201×3mm³ which is the same as in figure 3, and the aluminum material properties for peri-ultrasound modeling are listed in Table 1 along

with the material properties of inserted steel strips. Two identical cracks of length 19 mm and thickness d mm (d takes value 0, 1, 2 and 4 in this work) are considered for modeling damage growth. For wave propagation modeling, the setup for the transmitting point and the receiving points as well as numerical modeling process (calculation scheme, output variables etc.) are same as in section 3.2.

Table 2. Material properties of aluminum and steel used in peri-ultrasound modeling.

Materials	Young's modulus (GPa)	Poisson's ratio	Density (kg/m³)
Aluminum	71.50	0.33	2700
Steel	220.00	0.30	7800

# 5.2 Numerical modeling results

## 5.2.1 Numerical modeling and SPC-I analysis results

The peri-ultrasound modeling predicts wave motions over the entire 3-D problem geometry of the plate structure. Four cases with different crack thicknesses (0 mm, 1 mm, 2 mm and 4 mm) for the same crack length (19 mm) are numerically modeled. The snapshots of displacement magnitude fields at time steps  $16~\mu s$ ,  $20~\mu s$  and  $22~\mu s$ , for different crack thicknesses are shown in figure 12. These times are selected to show how elastic waves interact with these cracks as the wave fronts pass through the cracks.

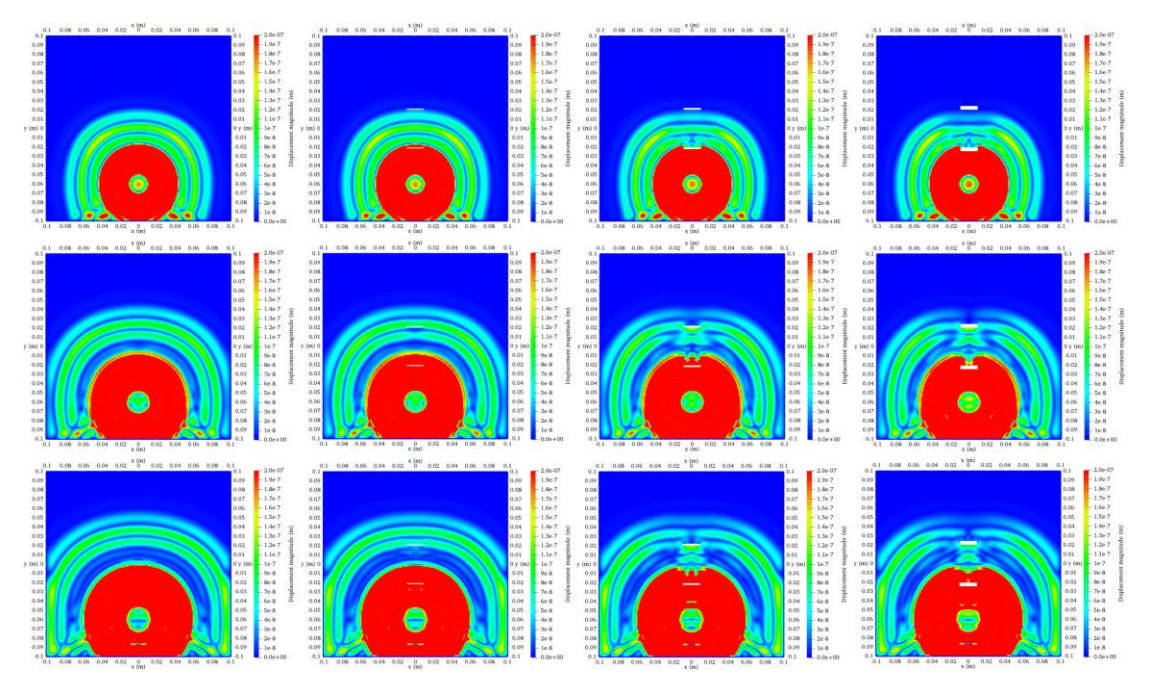
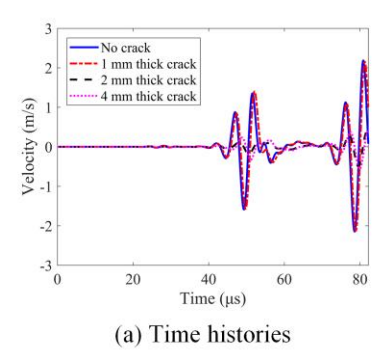


Figure 12. Wave motion snapshots in aluminum plates without any topography at different times in (1) plate containing no crack (the first column), (2) plate containing two 1 mm thick cracks (the second column), (3) plate containing two 2 mm thick cracks (the third column) and (4) plate containing two 4 mm thick cracks (the right column). Plots from top to bottom rows show wave fronts at times  $16 \mu s$ ,  $20 \mu s$  and  $22 \mu s$ .

It can be seen from figure 12 that peri-ultrasound modeling can successfully capture the wave propagation behaviors, and it also clearly shows the interactions between waves and cracks in the plate structures. At the receiving point, out-of-plane velocity fields for these four different crack thicknesses (0 mm, 1 mm, 2 mm and 4 mm) are recorded for further SPC-I analysis. The time histories and corresponding normalized spectral plots for the homogeneous aluminum plate are shown in figure 13.



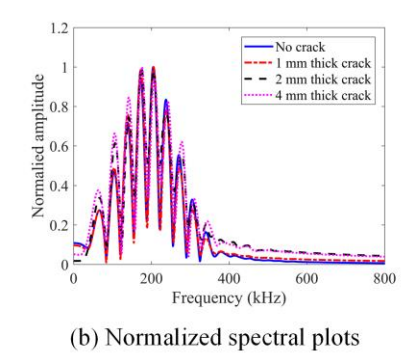
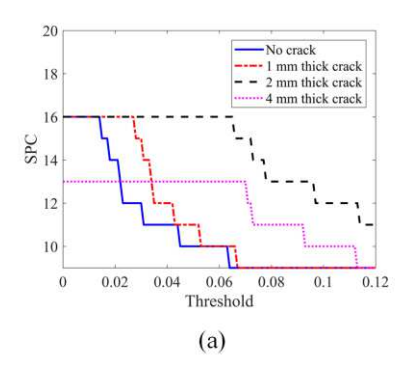


Figure 13. Time histories and normalized spectral plots for out-of-plane velocity fields in z direction at receiving point in the homogeneous aluminum plate.

Consider the spectral plots of figure 13b which are analyzed by the SPC-I technique. The SPC plots (number of peaks above the horizontal moving threshold line) are shown in figure 14a. The SPC-I values are the average of SPC values for all threshold positions and are shown in figure 14b.



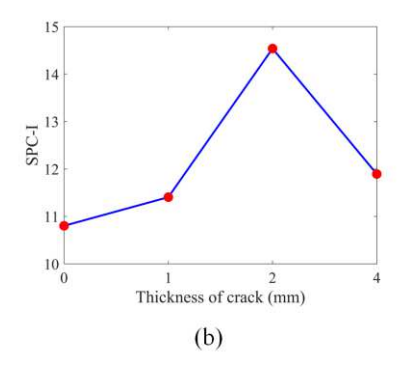


Figure 14. For the homogeneous aluminum plate, shown in figure 2b, containing two cracks of different thicknesses - 0 mm (no crack), 1 mm, 2 mm and 4 mm, the SPC plots with threshold varying from 0 to 12% of the maximum amplitudes of each spectral plot are shown in figure 14(a) and the SPC-I variations are shown in figure 14(b).

In several experimental and theoretical investigations this trend of SPC-I variation – first increasing and then decreasing, thus forming a hump has been reported [2, 11-13, 21-23]. Such hump in the SPC-I plot indicates the nonlinearity reaching the maximum value because of the highest density of macro-crack accumulation and then the SPC-I value starts to decrease as the

micro-cracks coalesce to form macro-cracks. Thus, such hump in the SPC-I plot can serve as a warning sign for macro-crack formation followed by coalescing of micro-cracks to form macro-cracks. In our modeling thicker cracks represent macro-cracks while thinner cracks are representative of micro-cracks since the acoustic energy can pass through the thinner cracks but not thicker cracks.

Wave propagation snapshots in the heterogeneous plate at times 16  $\mu$ s, 20  $\mu$ s and 22  $\mu$ s are shown in figure 15.

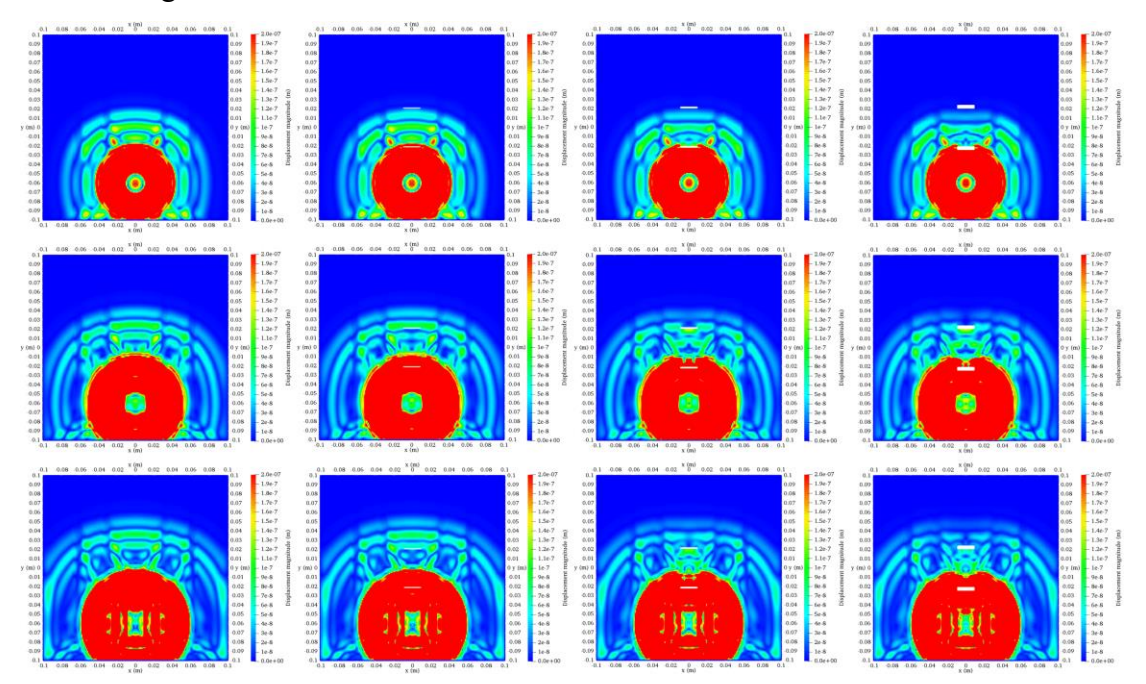


Figure 15. Wave motion snapshots in the heterogeneous plate structures with "X" topography at different times, (1) structure containing no crack (the first column), (2) structure containing two 1 mm thick cracks (the second column), (3) structure containing two 2 mm thick cracks (the third column) and (4) structure containing two 4 mm thick cracks (the right column). Plots from top to bottom rows show wave fronts at times 16 μs, 20 μs and 22 μs.

The time histories and corresponding normalized spectral plots for the heterogeneous plate are shown in figure 16. Following the same SPC-I analysis steps as in the homogeneous plate case, the SPC plots and SPC-I variations from the recorded signals are generated and shown in

figure 17.

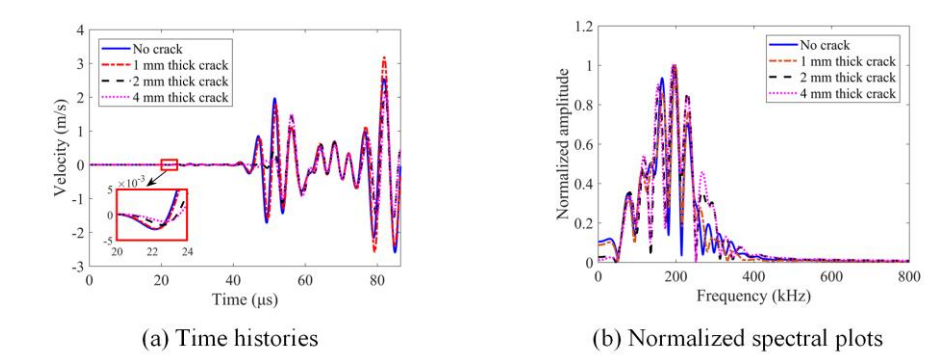


Figure 16. Time histories and normalized spectral plots for signals received on the receiving point in the plate structures with "X" topography.

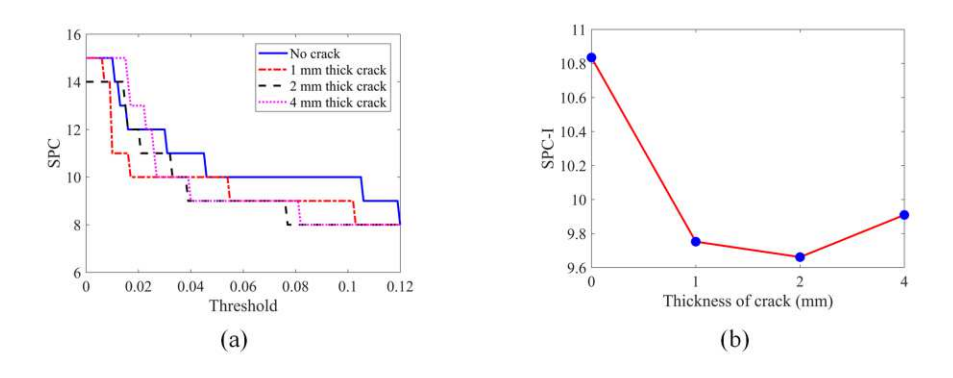


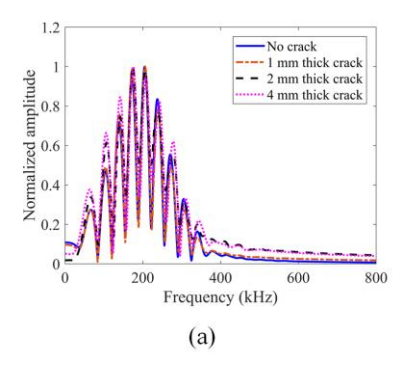
Figure 17. For the plate containing two cracks of different thicknesses and having "X" topography (vertical steel strips in an aluminum plate as shown in figure 11b) the SPC plots are shown in figure 17(a) and the SPC-I variations are shown in figure 17(b).

In the SPC-I results, since any hump is not noticed for the heterogeneous plate it can be concluded that "X" topography can hide cracks or make them undetectable when the SPC-I technique is used for their detection. Crack hiding phenomenon for "X" topography can be explained from the wave propagation plots presented above that show how wave energy interacts with cracks (see figures 12 and 15) as the wave passes through cracks. The existence of "X" topography in plate structures result in destructive interference between reflected waves from steel strips' boundary and the propagating wave from the source. After these mixed waves pass through cracks wave fronts cannot keep their perfect shapes and are made up of several

scattered clusters as shown in figure 15, and such scattered wave energy can cause nonlinear information lost at the receiving points making it difficult to monitor the damage growth. However, for the homogeneous plate, the wave front shape is not disturbed by such scattered energy after passing through cracks as shown in figure 12. Hence, the nonlinear information generated by the cracks is preserved in the propagating wave front and is recorded by the receivers making the damage growth detectable.

# 5.2.2 Spectral amplitude difference analysis

Here we analyze the differences in spectral plots between intact plate (without any cracks) and cracked plate for both homogeneous and heterogeneous structures. The spectral amplitude difference (SAD) is obtained from Fast Fourier transformed (FFT) normalized spectral plots by calculating the differences for each cracked case (0 mm, 1 mm, 2 mm and 4 mm) from the crack-free case (the reference case), and is used as an acoustic indicator for monitoring the damage evolution (increasing crack thickness here). The normalized spectral plots in figures 13b and 16b are replotted in figures 18a and 19a, respectively. From these normalized plots the SAD variations for both homogeneous and heterogeneous plates are obtained and shown in figures 18b and 19b, respectively.



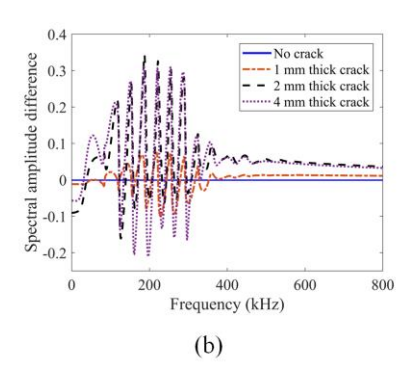
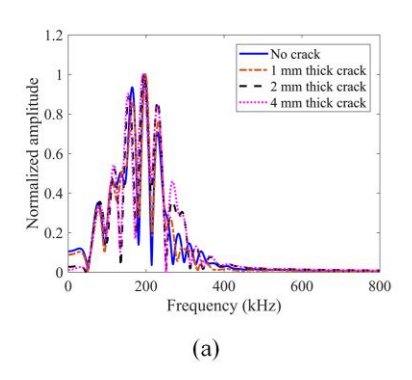


Figure 18. (a) Normalized spectral plots and (b) spectral amplitude difference plots for different thicknesses of cracks in homogeneous aluminum plate.



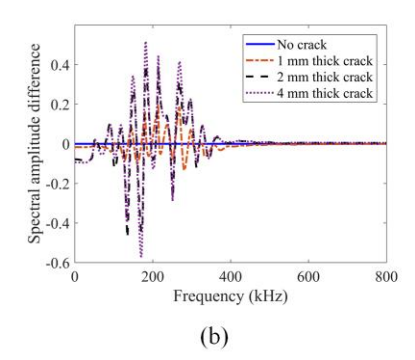


Figure 19. (a) Normalized spectral plots and (b) spectral amplitude difference plots for different thicknesses of cracks in the heterogeneous aluminum plate with "X" topography.

It can be seen from figures 18b that for the homogeneous aluminum plate the SAD parameter can distinguish cracks with thicknesses 0 mm, 1 mm and 2 mm but not for 2 mm and 4 mm at frequency ranges beyond around 100 kHz. Only within frequency around 100 kHz the SAD can show some distinctions for all crack thicknesses. For heterogeneous aluminum plate with "X" topography in the structure, the SAD only shows changes for these four thicknesses of cracks at the frequency range from approximately 150 kHz to 285 kHz as shown in figure 19b. At other frequencies there are not very clear and consistent changes for damage growth. The maximum relative changes (for 4 mm thick crack) from intact case (crack-free) can be around 35% for homogeneous plate as shown in figure 18b, and for "X" topography in the plate the maximum relative changes can approach to around 60% as shown in figure 19b. However, at higher frequencies, say around 400 kHz to 800 kHz the relative changes for these four crack thicknesses are very small for the heterogeneous case. Therefore, the SAD parameter can be an effective indicator for damage growth monitoring at certain frequency range.

# 6. Monitoring damage growth in topographical structures with topological acoustic sensing technique

In this section, an emerging concept – geometric phase change based on topological acoustics is adopted for monitoring damage growth in topographical structures. It is investigated whether the cracks that are hidden during SPC-I based monitoring can be detected

through geometric phase change parameter from topological acoustic sensing technique.

## 6.1 Topological acoustic sensing and geometric phase change

Topological acoustic sensing monitors the change in the geometric phase of an acoustic field (linear and/or nonlinear) as its vectorial representation is rotated in a multidimensional Hilbert space due to some perturbation. This phase is different from dynamic phase which is related to the phase accumulated by a wave as it travels at some speed along some path. The changes in vectorial representation of an acoustic field and its associated geometric phase relate to perturbation introduced in the reference system [29]. Previous studies that adopted topological acoustic sensing [30-34] show that any simple change in the medium supporting an acoustic field may cause significant changes in geometric phase. When the topology of the manifold in the multidimensional space spanned by the vectorial representation of an acoustic fields exhibits sharp topological features such as twists, small changes in the medium supporting the acoustic field may lead to a sharp jump in geometric phase. Monitoring changes around such features lead to the high sensitivity of the geometric phase to small perturbations.

First, we consider the acoustic fields in the homogenous plate with and without damages to illustrate the process of topological acoustic sensing. To illustrate the method of topological acoustic sensing, we consider a discretized subspace to describe the acoustic field. This subspace is constituted of seven receiving points as shown in figure 20. It should be noted that at least two receiving points are needed to reflect the spatial characteristics of the acoustic field. More receiving points will improve the spatial resolution of the acoustic field and its geometry. Here, seven points are distributed symmetrically about the y-axis as shown in figure 20a (for the homogeneous plate without any crack) and in figure 20b (for the homogeneous plate with two cracks). The geometric phase changes for the cracked plate compared to that with no crack case (reference state) because of the perturbations arising from these cracks. The thickness d of these two cracks takes values 0, 1, 2 and 4 mm for modeling damage growth in the plate. A plate having no crack is considered as the reference state or reference shape with respect to

which the cracked cases are compared.

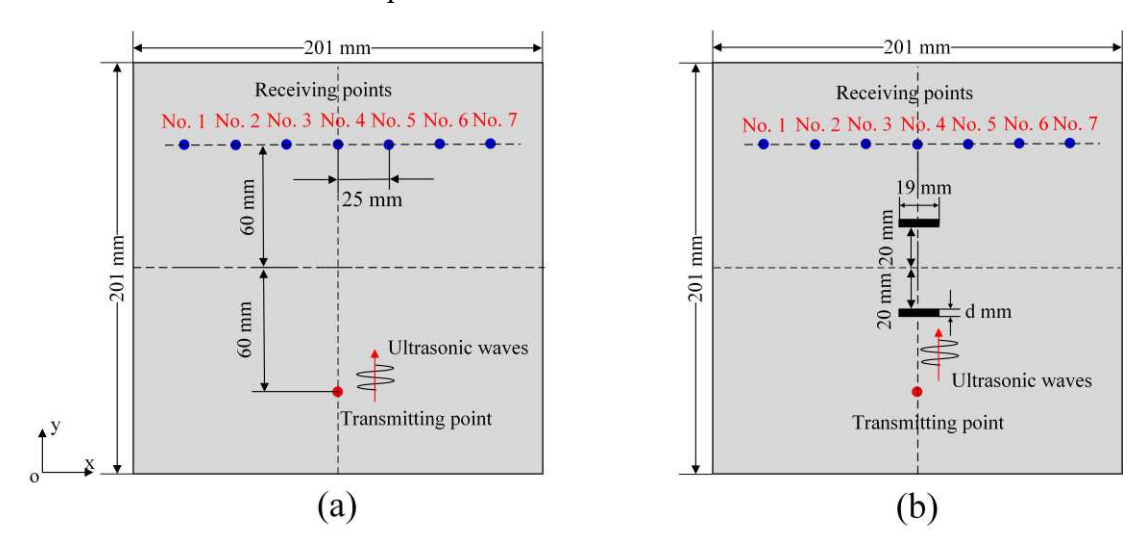


Figure 20. 2-D view of the problem geometry for geometric phase sensing (a) crack-free reference state and (b) cracked plate – perturbed state.

For the reference shape at each receiving location, we record the velocity as a time series. Each of these seven time histories are Fast Fourier transformed (FFT) to obtain complex amplitudes in the spectral domain. At a given frequency, these seven complex amplitudes can be represented as a normalized state vector in a seven-dimensional complex Hilbert space. The 7 basis vectors of that subspace correspond to locations in the physical space. This normalized state vector can be written as [34],

$$C = \frac{1}{\sqrt{C_1^2 + C_2^2 + C_3^2 + \dots C_7^2}} \begin{pmatrix} C_1 e^{i\phi_1} \\ C_2 e^{i\phi_2} \\ C_3 e^{i\phi_3} \\ \dots \\ C_7 e^{i\phi_7} \end{pmatrix}$$
(2)

In equation (2),  $C_i$  and  $\phi_i$  (i=1, 2, 3...7) are magnitude and spatial phase at each receiving point. The components of this multi-dimensional state vector are the complex amplitudes of the field at every location in the discretized space of the seven detectors. When cracks are introduced, the perturbation in the physical space scatters the acoustic waves and

modifies the spatial distribution of the acoustic field. Perturbations such as cracks then change the normalized complex amplitude of the acoustic field to,

$$C' = \frac{1}{\sqrt{C_1'^2 + C_2'^2 + C_3'^2 + \dots C_7'^2}} \begin{pmatrix} C_1' e^{i\phi_1'} \\ C_2' e^{i\phi_2'} \\ C_3' e^{i\phi_3'} \\ \dots \\ C_7' e^{i\phi_7'} \end{pmatrix}$$
(3)

At a single given frequency f, the angle between the vector representation of the acoustic field along the 7 locations in the crack-free and cracked systems corresponds to a change in the geometric phase of the acoustic wave. This angle or single geometric phase change at the given frequency f can be obtained from the dot product of these two state vectors and can be expressed as,

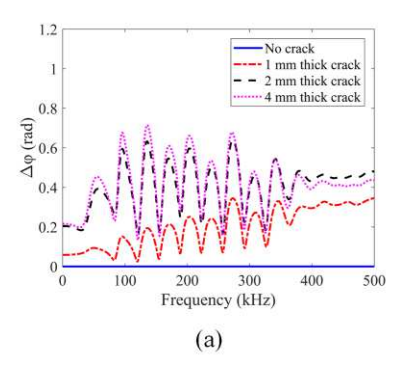
$$\Delta \varphi = \arccos\left(\operatorname{Re}\left(C^*\square C'\right)\right), \qquad \Delta \varphi \in [0, \pi]$$
 (4)

where  $C^*$  denotes the complex conjugate of state vector C while Re stands for the real part of a complex quantity.

Generally, the acoustic signals at each receiving point contain multiple frequencies, then a series of geometric phase changes can be plotted versus frequency. The spectral dependency of the geometric phase change  $\Delta \varphi$  measures changes in the spatial characteristics of the acoustic field during wave propagation due to perturbations.

# 6.2 Topological acoustic sensing results for damage growth

The damage growth monitoring results with topological acoustic sensing are presented in this section for both homogeneous and heterogeneous aluminum plates. Geometric phase changes are obtained from reference state vectors (crack-free plates) and perturbed state vectors from cracked plates for both homogeneous and heterogeneous aluminum plates. The effect of the crack growth in homogeneous and heterogeneous aluminum plates on the geometric phase change variations are shown in figures 21a and 21b, respectively.



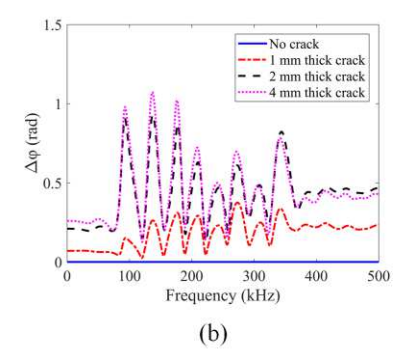


Figure 21. Geometric phase change as a function of frequency as the crack thickness increases in the homogeneous and heterogeneous aluminum plates (a) homogeneous plate and (b) heterogeneous plate.

In all plots shown in figure 21 one can see that the introduction of cracks and crack thickness variations have a strong effect on  $\Delta \varphi$  (the geometric phase change) for both homogeneous and heterogeneous plates. At certain frequencies the  $\Delta \varphi$  change is much stronger and show sharp peaks and dips compared to other frequencies. At higher frequencies (above around 400 kHz) the oscillations die down. However,  $\Delta \varphi$  can still distinguish between no crack, 1 mm thick crack and 2 mm thick crack cases. However, no significant difference between 2 mm and 4 mm thick cracks is noticed. It has been also shown here (see figure 14b) and in previous investigations [2, 11, 21] that SPC-I technique is more effective in sensing the initial stage of damage growth. At higher frequencies  $\Delta \varphi$  is showing a similar trend as SPC-I for these cracks.

It should be noted that the geometric phase change can sense the damage growth at the entire frequency range (0 to 500 kHz) while SAD only shows changes at limited frequency ranges. Moreover, for homogeneous aluminum plate the maximum relative changes of  $\Delta \varphi$  for 4 mm thick crack can be as high as around 70% as shown in figure 21a. For heterogeneous aluminum plate, this relative change can reach up to around 110% as shown in figure 21b which indicates that geometric phase change can show very high sensitivity for sensing damage growth in both homogeneous and heterogeneous aluminum plate structures.

#### 7. Discussions

In this work, an in-depth study investigating various nonlinear mechanisms affecting the newly developed sideband peak count-index (or SPC-I) technique is carried out. Three types of nonlinearity (material nonlinearity, structural nonlinearity and transducer-specimen contact nonlinearity) on sideband peak generations are investigated through both numerical modeling and experimental investigation. Both numerical modeling and experimental results show similar trends in sideband peak variations when ultrasonic waves propagate through nonlinear specimens. This investigation confirms that SPC-I technique captures nonlinear response in structures.

For material nonlinearity, sideband peak amplitudes vary but the main peak amplitudes remain same in the normalized spectral plots as the input signal amplitudes increase. For structural nonlinearity, presence of cracks in linear materials can affect the sideband peak amplitudes (typically they increase with the number of cracks and input signal amplitude). For contact nonlinearity at the transducer-specimen interface, sideband peak amplitudes show a decreasing trend in the normalized plot as the input signal amplitude increases. This trend has not been reported in the literature before. The contact nonlinearity effect is very weak compared to other types of nonlinearity and hence can be neglected in practical applications.

Three acoustic parameters – the nonlinear SPC-I value, spectral amplitude difference (SAD) and geometric phase change are then adopted for sensing damage growth in topographical structures. The SPC-I technique can sense such damage evolution in homogeneous aluminum plate without any topography, but cracks can remain hidden when "X" topography is introduced in the plate. The SAD parameter can monitor damage growth in both homogeneous and heterogeneous aluminum plate structures only at certain frequencies that highly depend on the Fast Fourier transform (FFT) plots and process. However, the proposed frequency-dependent geometric phase change parameter can sense damage growth in the entire frequency range with higher sensitivity compared to SAD parameter. Clearly, the geometric

phase change technique has some advantages for sensing damage evolution in complex structures.

#### 8. Conclusions

This work explains the nonlinear phenomenon when ultrasonic waves interact with different types of nonlinearity and how that nonlinearity is sensed by the SPC-I technique. Despite many success stories of experimental investigations with the SPC-I technique the existing literature has not provided a deeper understanding about how the nonlinear mechanism affects the SPC-I measurement. That knowledge gap is addressed in this paper. It explained why and how the SPC-I can capture the nonlinear response. Therefore, this work can provide a fundamental understanding of the SPC-I technique. For some heterogeneous structures, the damage growth can remain hidden to the SPC-I technique for which single transmitter-receiver pair is used. However, the geometric phase change obtained from multiple receivers can detect those cracks and monitor their growth with higher sensitivity compared to spectral amplitude difference (SAD) parameter.

## Acknowledgments

This work is partially supported by the National Science Foundation sponsored "New Frontiers of Sound Science and Technology Center" at the University of Arizona (Grant No. 2242925). Some financial support provided by the Central South University (CSU) in China towards the first author's stay in Arizona is also gratefully acknowledged.

#### References

- [1] Park S H, Kundu T. A modified sideband peak count based nonlinear ultrasonic technique for material characterization. Ultrasonics, 2023, 128: 106858.
- [2] Alnuaimi H, Amjad U, Russo P, et al. Monitoring damage in composite plates from crack initiation to macro-crack propagation combining linear and nonlinear ultrasonic techniques. Structural Health Monitoring, 2021, 20(1): 139-150.
- [3] Lan Z, Li W, Deng M, et al. Combined harmonic generation of feature guided waves mixing

- in a welded joint. Wave Motion, 2023, 117: 103103.
- [4] Jiang C, Li W, Ng C T, et al. Quasistatic component generation of group velocity mismatched guided waves in tubular structures for microdamage localization. Available at SSRN 4398162.
- [5] Li W, Jiang C, Xiao J, et al. Assessment of Thermal Damage in Polymethyl Methacrylate Using Quasi-static Components of Ultrasonic Waves. Journal of Nondestructive Evaluation, 2023, 42(1): 13.
- [6] Jiang C, Zhang C, Li W, et al. Assessment of damage in composites using static component generation of ultrasonic guided waves. Smart Materials and Structures, 2022, 31(4): 045025.
- [7] Jiang C, Li W, Deng M, et al. Quasistatic pulse generation of ultrasonic guided waves propagation in composites. Journal of Sound and Vibration, 2022, 524: 116764.
- [8] Zhang G, Li X, Li T, et al. Monitoring elastoplastic deformation in ductile metallic materials using sideband peak count-index (SPC-I) technique. Journal of Nondestructive Evaluation, Diagnostics and Prognostics of Engineering Systems, 2023: 1-15.
- [9] Wang, M., Pau, A., Zhang, G. et al. Monitoring prestress in plates by sideband peak count-index (SPC-I) and nonlinear higher harmonics techniques. Nonlinear Dynamics 111, 15749–15766 (2023).
- [10] Alnuaimi H N, Sasmal S, Amjad U, et al. Monitoring concrete curing by linear and nonlinear ultrasonic methods. ACI Materials Journal, 2021, 118(3).
- [11] Basu S, Thirumalaiselvi A, Sasmal S, et al. Nonlinear ultrasonics-based technique for monitoring damage progression in reinforced concrete structures. Ultrasonics, 2021, 115: 106472.
- [12] Castellano A, Fraddosio A, Piccioni M D, et al. Linear and nonlinear ultrasonic techniques for monitoring stress-induced damages in concrete. Journal of Nondestructive Evaluation, Diagnostics and Prognostics of Engineering Systems, 2021, 4(4): 041001.
- [13] Arumaikani T, Sasmal S, Kundu T. Detection of initiation of corrosion induced damage in

- concrete structures using nonlinear ultrasonic techniques. The Journal of the Acoustical Society of America, 2022, 151(2): 1341-1352.
- [14] Alnuaimi H N, Amjad U, Russo P, et al. Advanced non-linear ultrasonic sideband peak count-index technique for efficient detection and monitoring of defects in composite plates. Journal of Vibration and Control, 2023: 10775463231168228.
- [15] Alnuaimi H, Amjad U, Park S, et al. An improved nonlinear ultrasonic technique for detecting and monitoring impact induced damage in composite plates. Ultrasonics, 2022, 119: 106620.
- [16] Liu P, Sohn H, Kundu T, et al. Noncontact detection of fatigue cracks by laser nonlinear wave modulation spectroscopy (LNWMS). NDT & E International, 2014, 66: 106-116.
- [17] Park S H, Alnuaimi H, Hayes A, et al. Nonlinear acoustic technique for monitoring porosity in additively manufactured parts. Journal of Nondestructive Evaluation, Diagnostics and Prognostics of Engineering Systems, 2022, 5(2): 021008.
- [18] Hafezi M H, Alebrahim R, Kundu T. Peri-ultrasound for modeling linear and nonlinear ultrasonic response. Ultrasonics, 2017, 80: 47-57.
- [19] Hafezi M H, Kundu T. Peri-ultrasound modeling for surface wave propagation. Ultrasonics, 2018, 84: 162-171.
- [20] Hadi Hafezi M, Kundu T. Peri-ultrasound modeling of dynamic response of an interface crack showing wave scattering and crack propagation. Journal of Nondestructive Evaluation, Diagnostics and Prognostics of Engineering Systems, 2018, 1(1).
- [21] Zhang G, Li X, Zhang S, et al. Sideband peak count-index technique for monitoring multiple cracks in plate structures using ordinary state-based peri-ultrasound theory. The Journal of the Acoustical Society of America, 2022, 152(5): 3035-3048.
- [22] Zhang G, Li X, Kundu T. Ordinary state-based peri-ultrasound modeling to study the effects of multiple cracks on the nonlinear response of plate structures. Ultrasonics, 2023, 133: 107028.

- [23] Zhang G, Li X, Li T, et al. Ordinary state-based peri-ultrasound modeling for monitoring crack propagation in plate structures using sideband peak count-index technique. Journal of Sound and Vibration, 2024, 568: 117962.
- [24] Martowicz A, Packo P, Staszewski W J, et al. Modelling of nonlinear Vibro-acoustic wave interaction in cracked aluminum plates using local interaction simulation approach[C]//6th European Congress on Computational Methods in Applied Sciences and Engineering, Vienna, Austria. 2012.
- [25] Delsanto P P, Scalerandi M. A spring model for the simulation of the propagation of ultrasonic pulses through imperfect contact interfaces. The Journal of the Acoustical Society of America, 1998, 104(5): 2584-2591.
- [26] Shen Y, Cesnik C E S. Modeling of nonlinear interactions between guided waves and fatigue cracks using local interaction simulation approach. Ultrasonics, 2017, 74: 106-123.
- [27] Shen Y, Cesnik C E S. Nonlinear scattering and mode conversion of Lamb waves at breathing cracks: An efficient numerical approach. Ultrasonics, 2019, 94: 202-217.
- [28] Zhang G, Hu B, Alnuaimi H, et al. Numerical modeling with experimental verification investigating the effect of various nonlinearities on the sideband peak count-index technique. Ultrasonics, 2024: 107259.
- [29] Banerjee S. Metamaterials in Topological Acoustics. CRC Press, 2023.
- [30] Lata T D, Deymier P A, Runge K, et al. Topological acoustic sensing of spatial patterns of trees in a model forest landscape. Ecological Modelling, 2020, 419: 108964.
- [31] Lata T D, Deymier P A, Runge K, et al. Topological acoustic sensing of ground stiffness: Presenting a potential means of sensing warming permafrost in a forest. Cold Regions Science and Technology, 2022, 199: 103569.
- [32] Lata T D, Deymier P A, Runge K, et al. Topological acoustic sensing using nonseparable superpositions of acoustic waves. Vibration, 2022, 5(3): 513-529.
- [33] Hasan M A, Deymier P A. Modeling and simulations of a nonlinear granular metamaterial:

application to geometric phase-based mass sensing. Modelling and Simulation in Materials Science and Engineering, 2022, 30(7): 074002.

[34] Lata T D, Deymier P A, Runge K, et al. Underwater acoustic sensing using the geometric phase. The Journal of the Acoustical Society of America, 2023, 154(5): 2869-2877.